Supplementary Information (SI) for Materials Horizons.

Supporting Information

Dissolvable Molecule Bridges Promoting Buried Interface Modification for High-Performance Inverted Perovskite Solar Cells

Ruixiong Hu,[a] Likai Zheng,[b] Huang Bin,[a] Yimin Xuan[a,*]

[a] School of Energy and Power Engineering, Nanjing University of Aeronautics and Astronautics, Nanjing 210016, P. R. China.

[b] Laboratory of Photonics and Interfaces, École polytechnique fédérale de Lausanne, 1015 Lausanne, Switzerland.

[*] Corresponding Author: E-mail address: ymxuan@nuaa.edu.cn (Y.M. Xuan)

Materials

Methylammonium iodide (MAI), formamidinium iodide (FAI), and methylammonium chloride (MACl), purchased from Greatcell Solar Materials. 4-Fluorobenzylphosphonic acid (4F-BPA), Benzylphosphonic acid (BPA), Cesium iodide (CsI), 2-propanol (IPA, anhydrous, 99.5%), chlorobenzene (anhydrous, 99.8%), N,N-dimethylformamide (DMF, anhydrous 99.8%), and dimethyl sulfoxide (DMSO, >99.5%) were purchased from Sigma Aldrich. Lead iodide (PbI_2), 3(methylthio) propylamine hydroiodide (3MTPAI), propane-1,3-diammonium iodide ($PDAI_2$), C_{60}, and Bathocuproine (BCP) were purchased from Xi'an Polymer Light Corp. [2-(9H-Carbazol-9-yl)ethyl]phosphonic Acid (2PACz), [4-(3,6-Dimethyl-9H-carbazol-9yl)butyl]phosphonic Acid (Me-4PACz), and Propylphosphonic acid (PPA) were purchased from TCI Chemicals. Nickel oxide nanoparticles (NiO_x) were purchased from Liaoning Advanced Technology. All chemicals were used as received without any other purification.

Device Fabrication

The FTO glass substrates were cleaned with detergent water, deionized water and ethyl alcohol each for 20 min in an ultrasonic bath. After being dry by nitrogen flow, the cleaned FTO substrates were stored in a hot oven under 110 °C overnight. Before use, the substrates were treated by ozone-ultraviolet for 15 min.

NiOx nanoparticles (7 mg/mL in deionized water) were spin-coated at 3000 rpm for 30 s on the FTO substrates, then annealed at 130°C for 30min in air. Then the samples were transferred immediately into a N_2-filled glove box (O_2<0.01 ppm, H_2O<0.01 ppm). The SAM layer was fabricated by using the mixed SAM solution of 2PACz and Me-4PACz in ethanol, the concentration for 2PACz and Me-4PACz was 0.17 mg/ml and 0.33 mg/ml, respectively. The SAM in ethanol solution was spin-coated on NiOx layer at 3000 rpm for 30 s, followed by annealing at 120 °C for 10 min. The temperature of the N_2-filled glove box for the deposition of DMB and the perovskite layer need to be controlled under 22°C. The DMBs (4F-BPA, BPA and PPA) were dissolved in ethanol for different concentrations. The DMB layer was deposited on the SAM layer via dynamic spin-coating 100 μL DMB solution at 3000 rpm for 30 s, then dried the wet film at 120 °C for 1 min. For control groups, this step was replaced by spin-coating 100 μL pure ethanol at 3000 rpm for 30 s, then dried the wet film at 120 °C for 1 min.

The perovskite solution was prepared by dissolving 15 mg MACl, 0.075 mmol CsI, 0.15 mmol MAI, 1.275 mmol FAI, and 1.5 mmol PbI_2 in 900 μL mixed DMF and DMSO solution (745 μL DMF + 155 μL DMSO), and additional 4% PbI_2 were added to the precursor to improve the crystallization. The precursor was stirred at 25 °C for 3 h, and filtered with a PTFE filter (0.2 μm) before use. For perovskite layer used in long-term stability test, $Cs_{0.05}FA_{0.95}PbI_3$ perovskite precursor was prepared by dissolving CsI, PbI_2, FAI in chemical ratio. 15 mol% additional MACl was added to improve film quality.

For Perovskite layer deposition, at around 90 μL filtered precursor was dropped on the HTL. To ensure the dissolvement of the DMB layer, we strongly recommend to ramp for 5 s, to wait for the precursor slowly cover the whole substrate. We also recommend to spread the precursor with a clean pipette gun head, but a 5 s ramp time was still necessary. Then the precursor was spin-coated at 1000 rpm for 10 s (acceleration rate 500 rpm/s) and 5000 rpm for 35 s (acceleration rate 1000 rpm/s), respectively. At the last 15 s of the second step, 150 μL anisole was dropped as antisolvent. The wet, dark colored films were transferred to a 120 °C hotplate and annealed for 20 min. For perovskite layer used in long-term stability test, at the last 5s of the second step, 300 μL EA was dropped as antisolvent, the wet, dark colored films were transferred to a 100 °C hotplate and annealed for 30 min.

For passivation, we used a bimolecular passivation (BMP) treatment following the procedures reported by Bin Chen, et al[1,2]. 0.2 mg $PDAI_2$ and 0.28 mg 3MTPAI were dissolved in a mixed solvent (500 μL CB and 500 μL IPA), then dynamically spinning-coated on the perovskite surface at 4000 rpm for 28 s, followed by annealing at 100 °C for 5 min.

For ETLs, 25 nm C_{60} and 7 nm BCP were thermally evaporated on the perovskite films at a rate of 0.2 A/s under a high vacuum of ~10^{-4} Torr. Finally, 140 nm Ag electrode was evaporated by thermal evaporation at a rate of 0.1 A/s for first 200 nm, and 1 A/s for the rest. For perovskite layer used in long-term stability test, BCP were replaced by 22 nm SnO_2 deposited by ALD system, and Ag contact was replaced by 80 nm Au.

Characterization

The J-V curves of PSCs were measured by a Keithley 2400 source meter under AM1.5G illumination with a solar simulator (CROWNTECH, EASISOLAR-160-3A) with a scan rate of 50 mV/s. The intensity of 1000 W/m^2 was calibrated by a standard silicon reference solar cell (CROWNTECH). The PSCs were masked using a shadow metal mask to limit the active cell area to 0.16 cm^2. The EQE spectra were measured by a CROWNTECH system (QTEST HIFINITY 5) and was calibrated by a certified silicon cell (CROWNTECH) before measurement. The atomic force microscopic (AFM) and Kelvin probe force microscopy (KPFM) images were performed by an atomic force microscope (NX-Hivac, Park). The profile images and top-view images of the perovskite films and PSCs were obtained by a field-emission scanning electron microscopy (FESEM; ZEISS, Gemini SEM300). The spectral characteristics were obtained by a UV-Vis-NIR spectrophotometer (PerkinElmer, Lambda 1050+). The X-Ray Diffraction measurements were conducted by an X-ray diffractometer (BRUKER, D8 ADVANCE). The ultraviolet photoelectron spectra were obtained by a photoelectron spectrometer (Thermo Fisher Scientific, EscaLab 250Xi) with a He-discharge lamp ($h\nu$=21.22 eV). Steady-state and time-resolved photoluminescence (PL) spectra were obtained by a photoluminescence spectrometer (Edinburgh, FLS-1000). The steady-state PL measurements were conducted with a Xenon lamp light source and the time-resolved PL measurements were conducted with a pulsed diode laser (EPL) light source of 405 nm. The EIS measurements, TPV measurements, capacitance-frequency (C-F) measurements of the PSCs were conducted by Paios (Fluxim, Switzerland). The liquid-state 1H NMR measurements were conducted in DMSO-d6 using a Bruker 400 MHz measurement spectrometer. The XPS spectroscopy was obtained by using the Thermo Scientific ESCALAB 250Xi system. For TOF-SIMS measurements, the IONTOF M6 instrument was utilized with the pulsed primary ions from the ion beam (1 keV) for sputtering and a Bi^{3+} pulsed primary ion beam for analysis.

Supplementary Note 1: The residual stress within the perovskite layer

The residual stress within the perovskite layer was measured by grazing incidence XRD (GIXRD) technique, conducted by an X-ray diffractometer (BRUKER, D8 ADVANCE) with a grazing incidence module (Cu, $\lambda = 1.54$ Å). The perovskite layers deposited on HTLs w/ & w/o 4F-BPA were first sent for XRD measurement, the 2θ scan range was set from 10° to 45°, to identify the (210) crystal panel of the perovskite layer (at around 30°~32°). Then, change the 2θ scan range to 30° to 35°, and measure the XRD patterns of the perovskite layer under various tilt angles from 0~50° ($\Psi = 0, 10, 20, 30, 40, 50°$), to get the X-ray diffraction images of perovskite at different depths. The GIXRD patterns of each tilt angles were collected, then found the abscissas (2θ value) of the ***peak*** in each (210) crystal panel under various tilt angles as shown in Fig.4g and 4f. The interplanar spacing values of each (210) crystal panel were calculated by the following formula:

$$d_n = \frac{\lambda}{2\sin\theta}$$

where $\lambda = 1.54$ Å of incident X-ray, θ was calculated from the 2θ values of the peak in each (210) crystal panel. As shown in Fig. 4i, the d_n values of each tilt angle Ψ were further plotted into scatter plot with corresponding $\sin^2 2\Psi$ values as abscissas.

The residual stress in the perovskite film was evaluated by the following formula:

$$\sigma_R = \left(\frac{E}{1+\upsilon}\right)\left(\frac{m}{d_n}\right)$$

where σ_R was the residual stress of the film; E is Young's modulus of the perovskite film (15 GPa); υ was the Poisson's ratio (0.3); m is the slope of the straight line after linear fitting in Fig. 4i; d_n is the intercept of the straight line after linear fitting in Fig. 4i.

Moreover, ***repeated experiments*** were conducted. As shown in Fig. SN1, the control film presented a slope with positive value, suggesting the presence of tensile stress within the layer. On the contrary, the perovskite film deposited on 4F-BPA modified HTL showed a small negative slope, indicating the presence of compression stress. Further calculation discovered the residual stress value for control and 4F-BPA treated film were 44.89 MPa and -4.02 MPa, respectively. The results showed good similarity to the previous results, confirming the validity of the experimental methodology and the reproducibility of the DMB strategy.

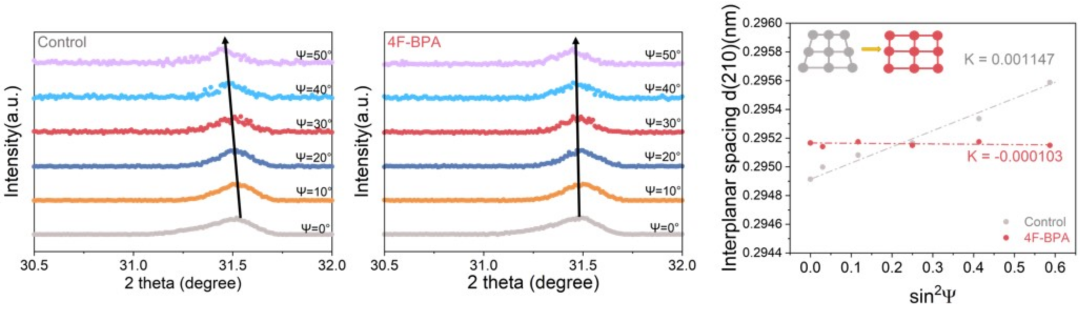

Figure SN1 for ***repeated*** experiments: a) GIXRD spectra for perovskite film deposited on control HTL and b) HTL treated by 4F-BPA. c) Leaner fitting curve for GIXRD data.

Supplementary Note 2: Peel off the perovskite layer deposited on a High-haze rough FTO substrate

We noted that the peel-off strategy had been widely applied in various studies, to explore the physical and chemical properties of the perovskite buried interfaces. These methods were mostly achieved by applying UV glue on perovskite surface and attached a clean ITO substrate on it. After the glue was hardened by UV light, the buried interface was exposed for characterization by peeling of the top ITO substrate. However, for most inverted perovskite solar cells deposited on high-haze rough FTO substrate, it was difficult to peel off a relatively complete perovskite layer.

Here we proposed a pressure-introduced peeling-off method for the Perovskite layer deposited on FTO substrate. We noted that introducing pressure during the UV glue hardening process was necessary, after carefully studied the variation between the film integrity, pressure, and hardening time, we found a pressure for 10 N/cm^2, 15 min hardening time was suitable, and could easily be achieved by applying a butterfly clip. Following steps would be helpful:

First prepared a clean FTO substrate and cut it into a 2.5 cm*1 cm piece. Then drop about 10 μL of UV glue (NOA #63) on it, and carefully put it on the perovskite film. Afterwards, apply a butterfly clip on these two glasses, use a UV light (465 nm) for 15 min hardening. Changing the position of the clip was also necessary for complete hardening. Finally, insert a blade into the gap between the two pieces of glass, and could easily peel off a relatively large perovskite film for further characterization.

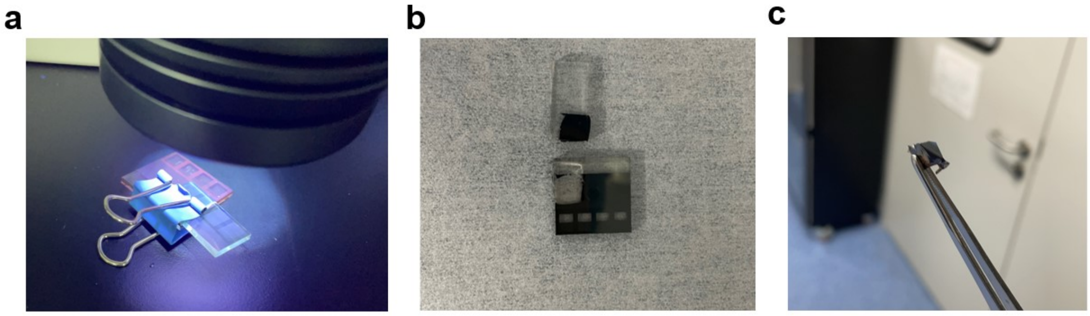

Figure SN2: Instructions for peeling off perovskite film from a rough high haze FTO substrates

Supplementary Note 3: Computational details

All calculations were carried out with CP2K package (version 7.1) in the framework of the density functional theory [3], based on the hybrid Gaussian and plan-wave scheme[4]. Molecular orbitals of the valence electrons were expanded into DZVP-MOLOPT-SR-GTH basis sets[5], and the exchange-correlation between the electrons were treated by employing the Predew-Burke-Ernzerhof (PBE) functional supplemented with the Grimmes D3 dispersion correction. The interaction between the valence electrons and atomic cores were described by the norm-conserving Goedecker-Teter-Hutter (GTH) pseudopotentials. A plane-wave density cutoff of 500 Ry was adopted. All the structures fully relaxed by CP2K with BFGS scheme, and the force convergence criterion was set to $4.5 * 10^{-4}$ hartree/bhor. The Brillouin zone integration is performed using a 2x2x1 k-mesh. A vacuum layer of 15 Å is added perpendicular to the sheet to avoid artificial interaction between periodic images.

Supplementary Figures:

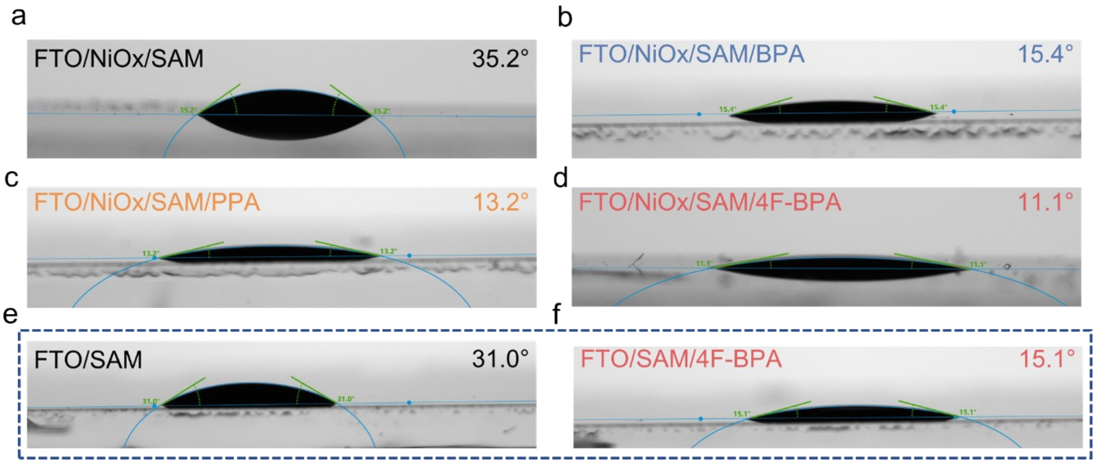

Figure S1: Contact angle for perovskite precursor on a) control HTL, and HTLs treated by DMBs, b) PPA, c) BPA, and d) 4F-BPA, respectively. e) Contact angle for perovskite precursor on FTO/SAM based HTL, and f) FTO/SAM based HTL treated by 4F-BPA as DMB.

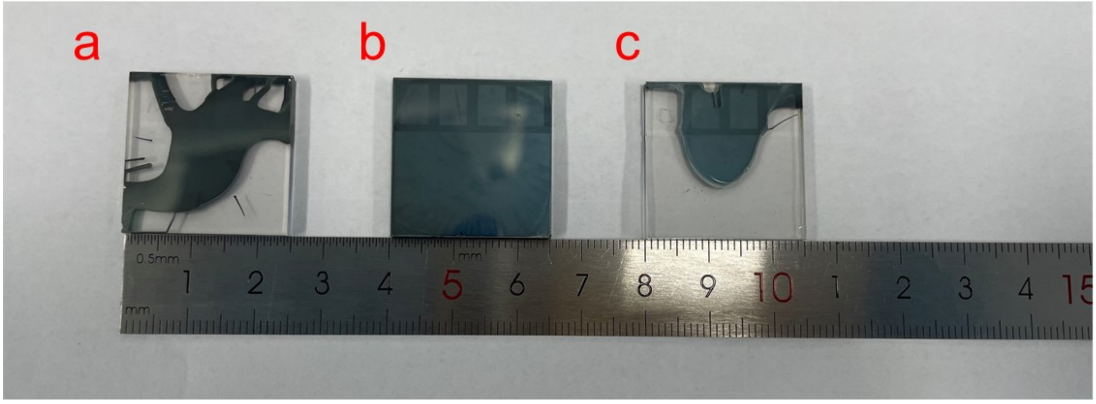

Figure S2: Perovskite film deposited on a) control HTL and b) HTL treated by 4F-BPA as DMB. c) Perovskite film with 4F-BPA as additive deposited on control film.

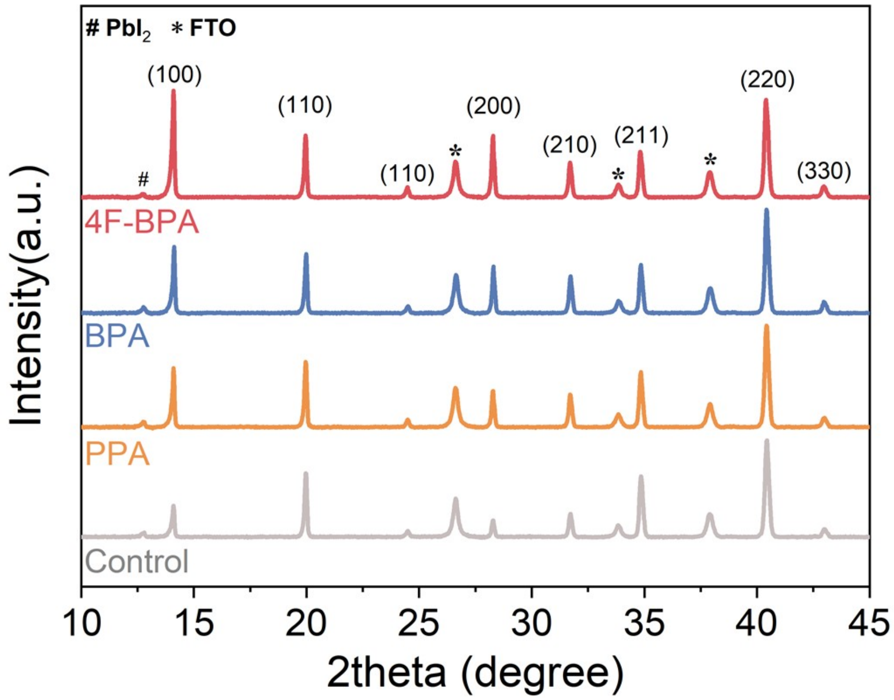

Figure S3: High-resolution figures for XRD patterns shown in Fig. 1g.

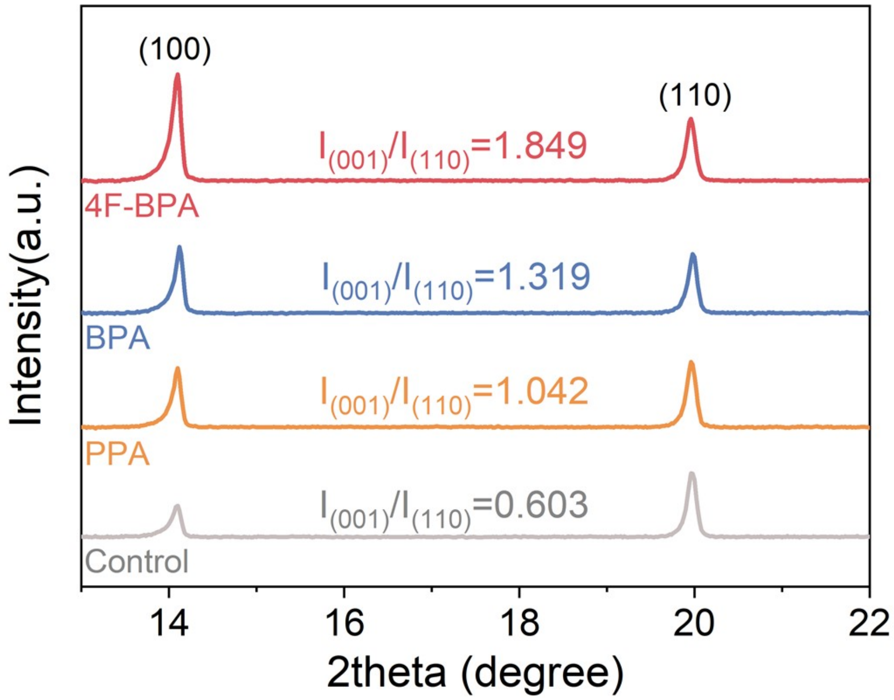

Figure S4: XRD peak intensity for (001) and (110) crystal panels.

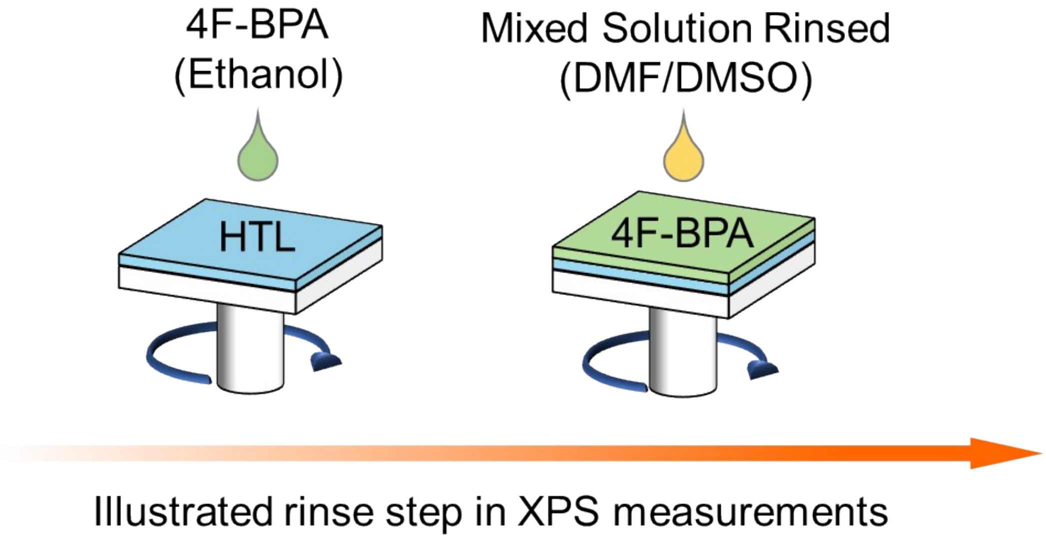

Figure S5: Illustration figure for DMF/DMSO rinsed step in XPS measurements

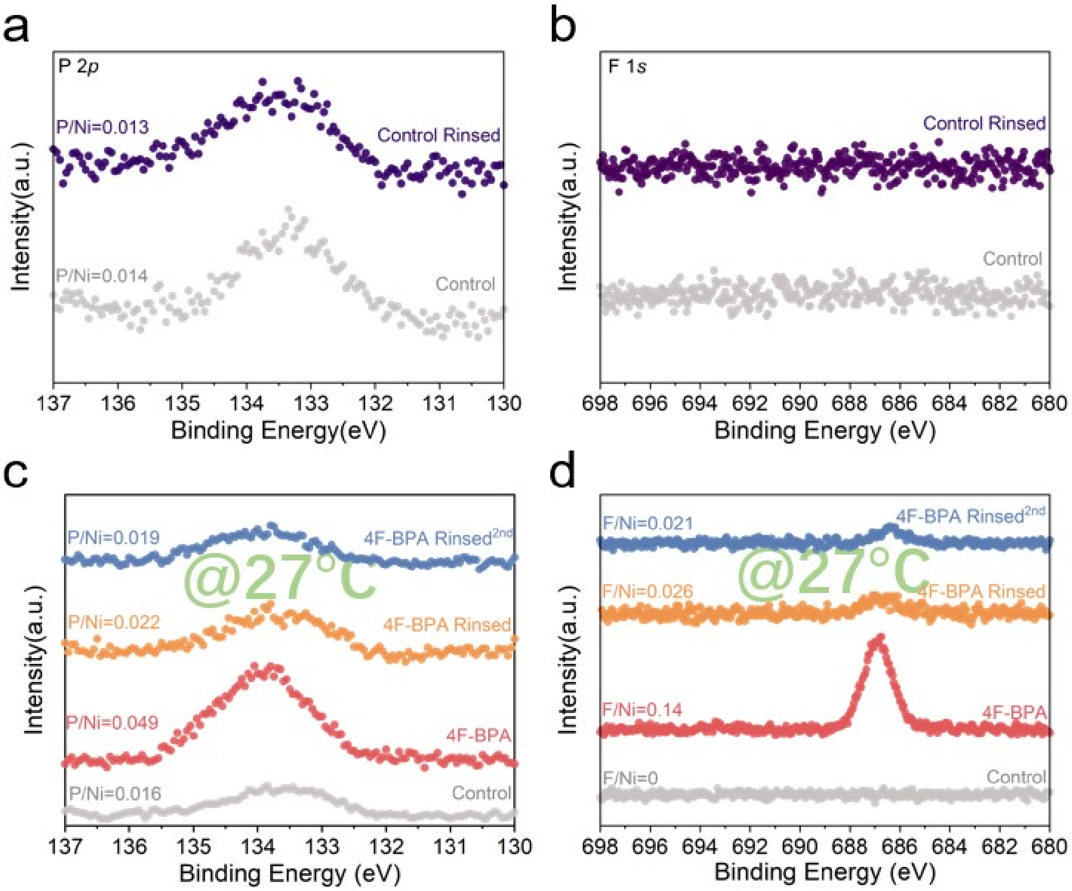

Figure S6: a) Relative P/Ni and b) F/Ni XPS intensity for control HTL and control HTL rinsed by DMF/DMSO solution. c) Relative P/Ni and d) F/Ni XPS intensity for HTLs treated by 4F-BPA, then rinsed by DMF/DMSO solution, whole process carried out in a 27 °C N_2-filled glove box.

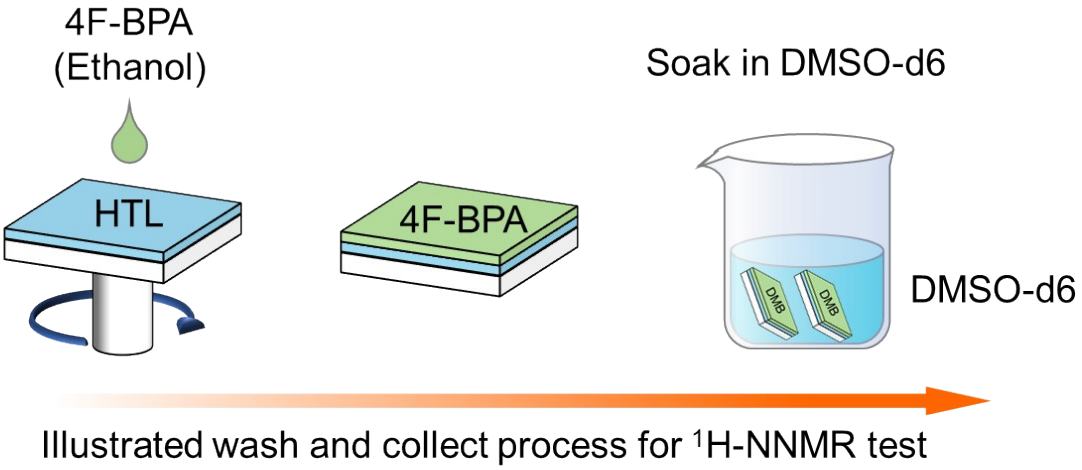

Figure S7: Illustration figure for wash and collect process in ^{1}H-NNMR test

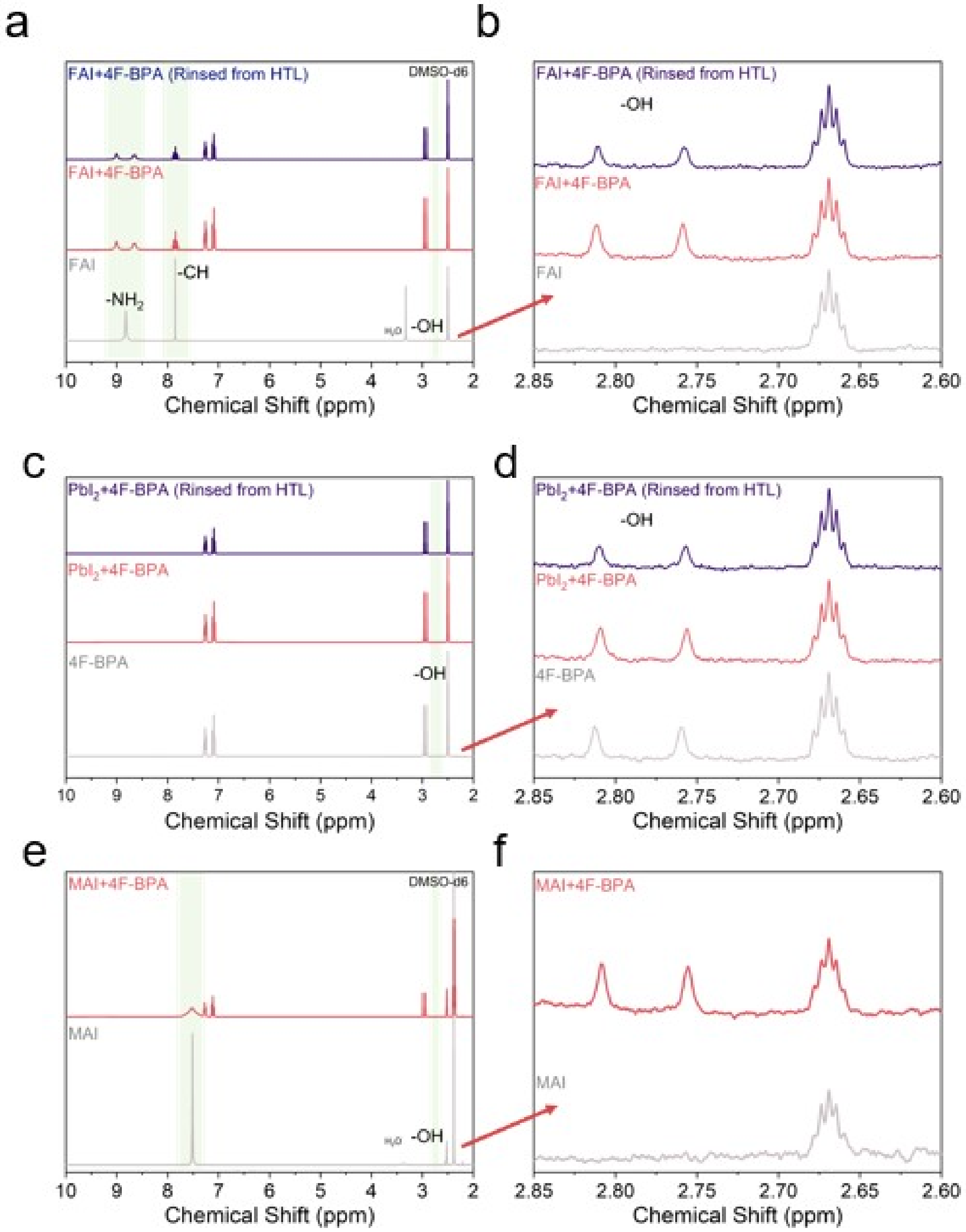

Figure S8: a) and b) ^{1}H NMR spectra for FAI, and FAI incorporated with 4F-BPA. c) and d) ^{1}NMR spectra for PbI_2, and PbI_2 incorporated with 4F-BPA. e) and f) ^{1}NMR spectra for MAI, and MAI incorporated with 4F-BPA.

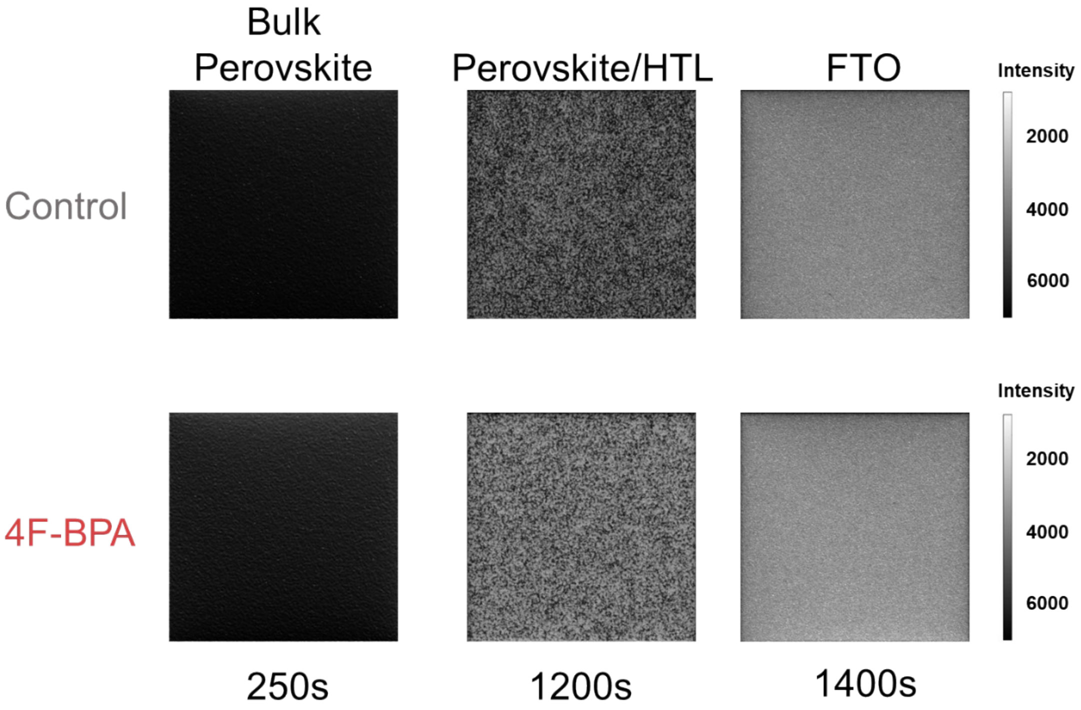

Figure S9: TOF-SIMS optical microscopes with various sputter time.

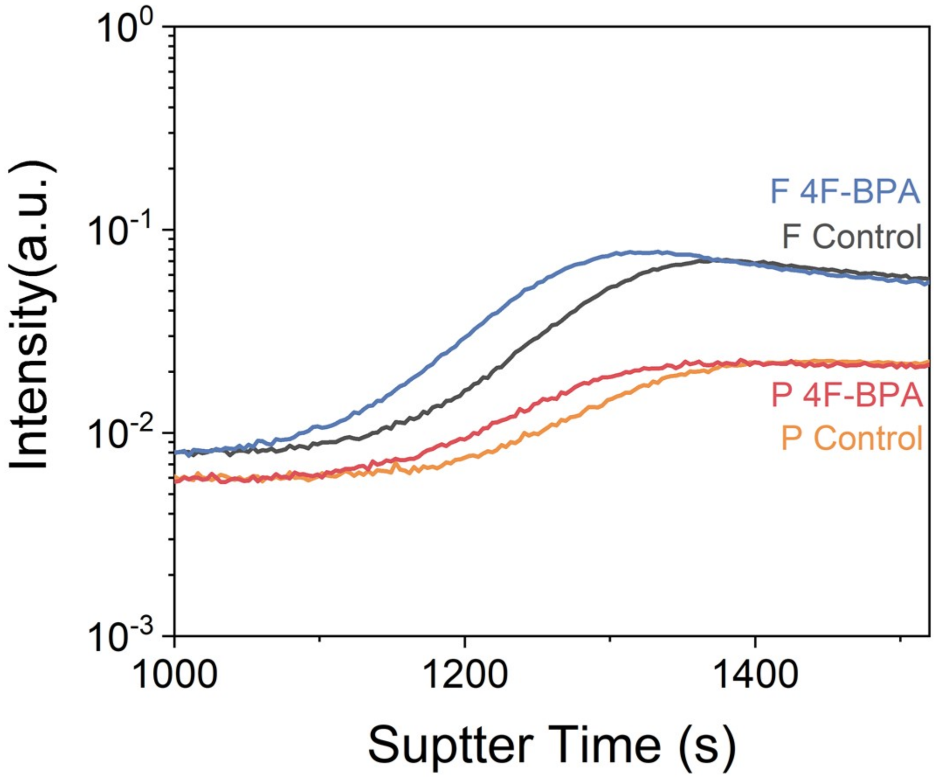

Figure S10: TOF-SIMS depth profile for F and P elements for perovskite layer w/&w/o 4F-BPA as DMB.

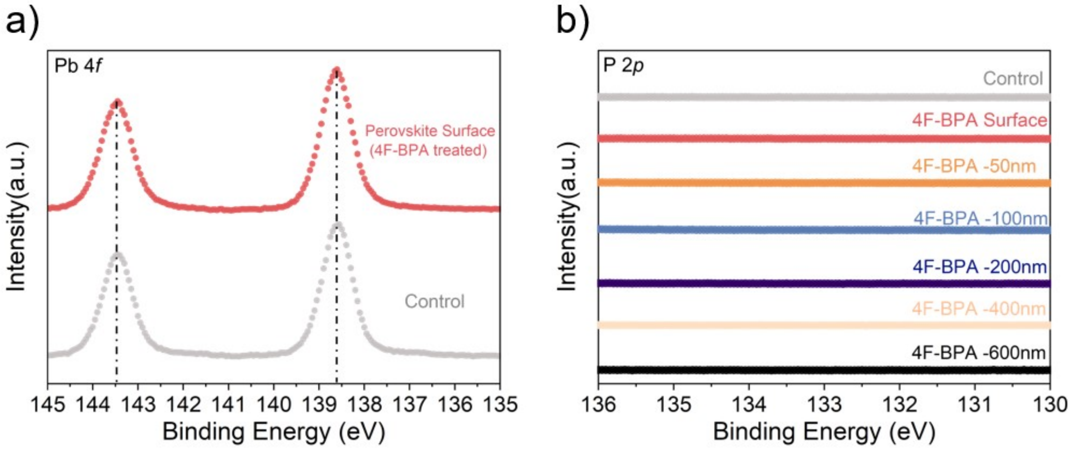

Figure S11: a) Pb 4f XPS spectra of the perovskite film surface and b) P 2p depth-profile for perovskite films with HTL treated by 4F-BPA.

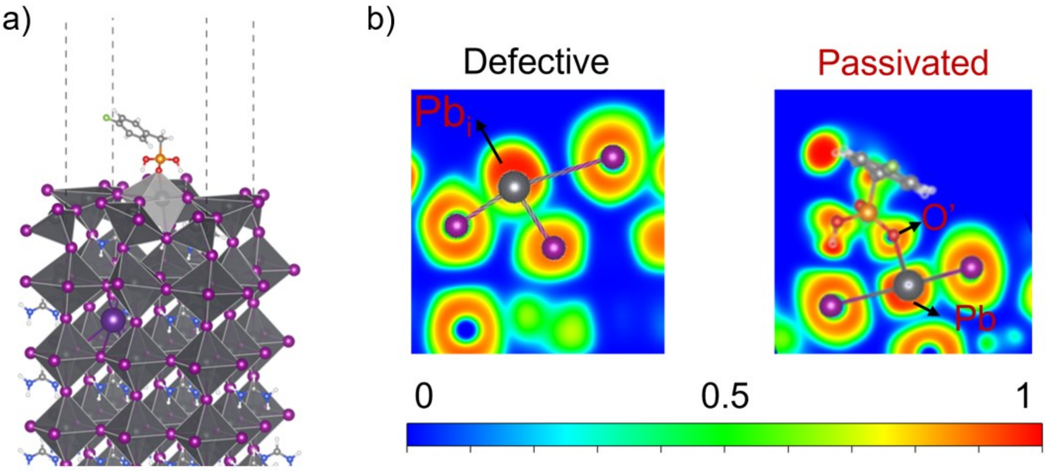

Figure S12: a) The absorption structure of 4F-BPA with the perovskite surface. b) the electron localization function in the region of the defective molecular configuration and the passivated molecular configuration

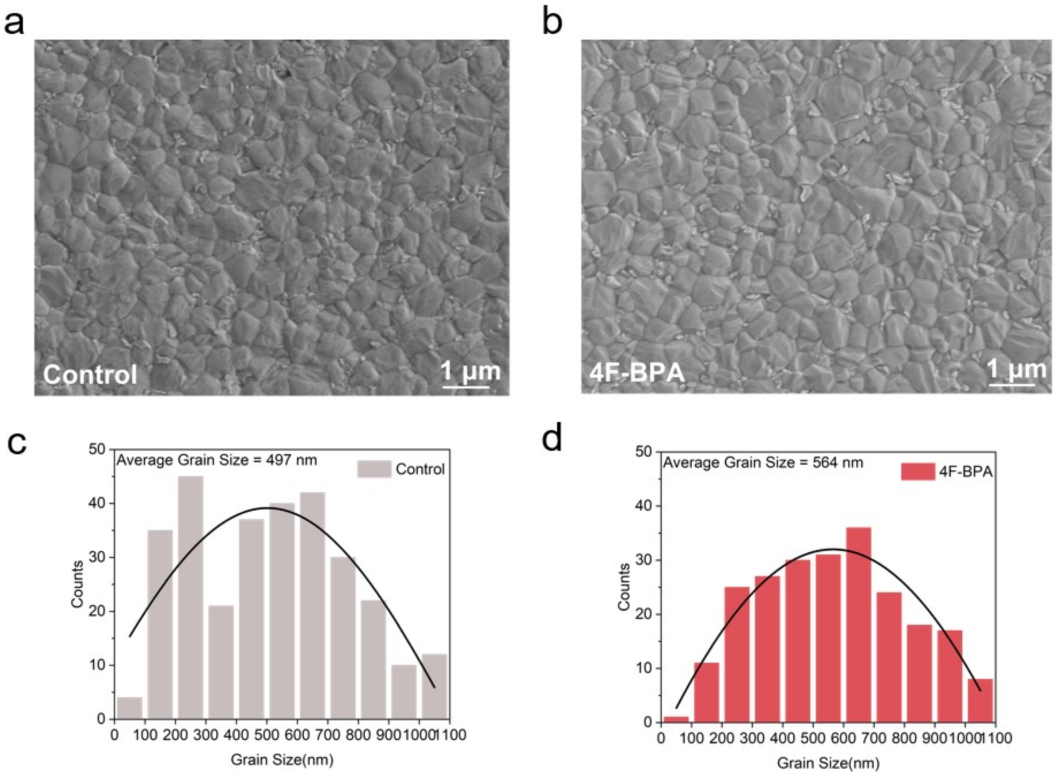

Figure S13: a) SEM images for perovskite surface on control HTL and b) on 4F-BPA treat HTL. c) grain size charts for perovskite layer on control HTL and d) on 4F-BPA treat HTL.

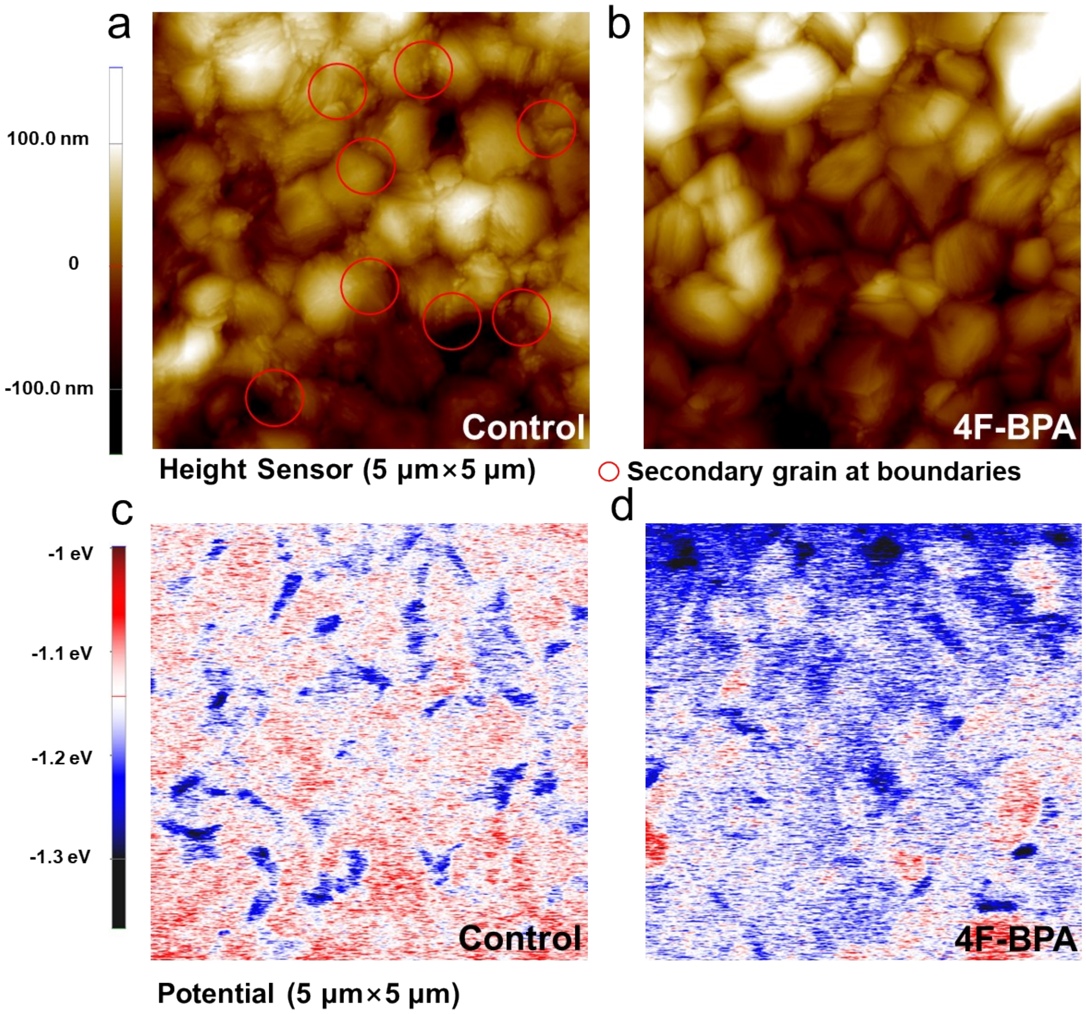

Figure S14: a) AFM images for perovskite surface on control HTL and b) on 4F-BPA treat HTL. c) KPFM images for perovskite surface on control HTL and d) on 4F-BPA treat HTL.

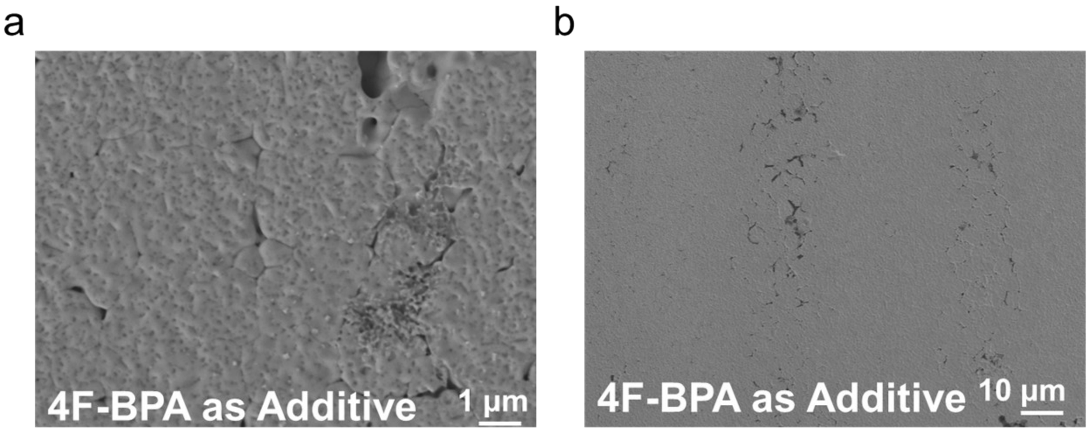

Figure S15: SEM images for the buried interface of Perovskite layer with 4F-BPA as additive, deposited on control HTL.

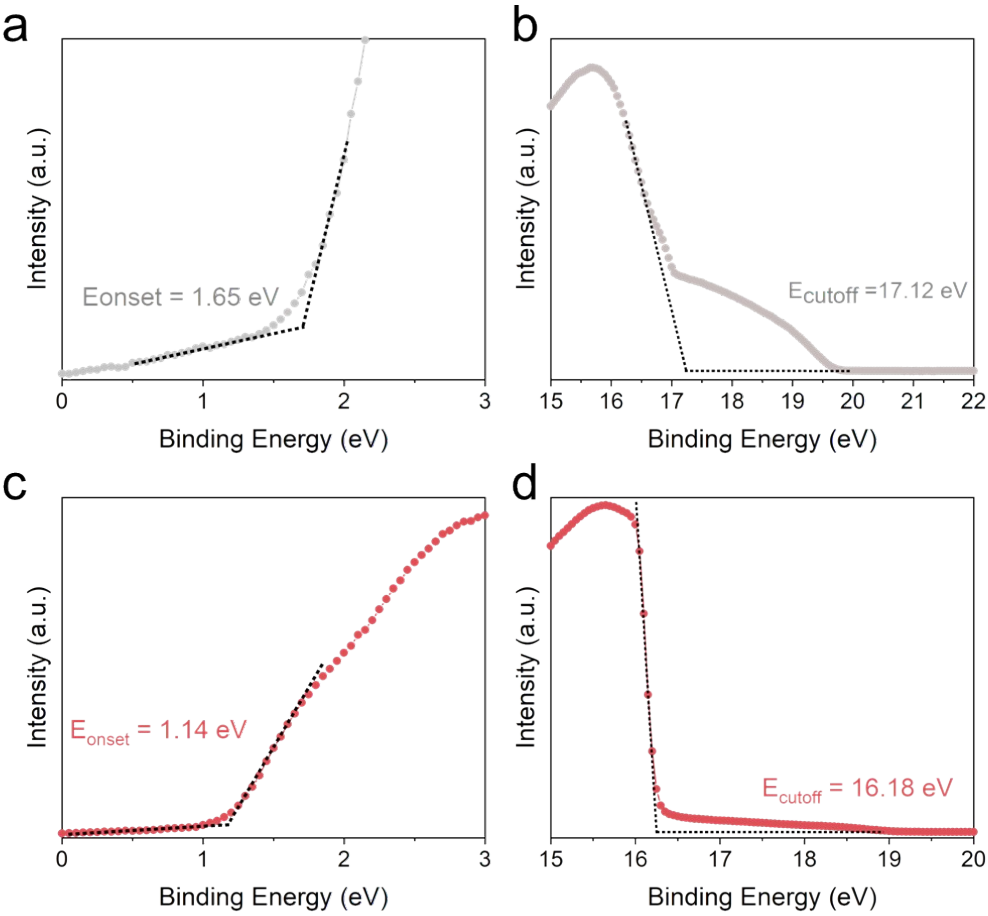

Figure S16: a) and b) UPS spectra for the buried interface of perovskite film deposited on control HTL. c) and d) UPS spectra for the buried interface of perovskite film deposited on HTL modified by 4F-BPA as DMB.

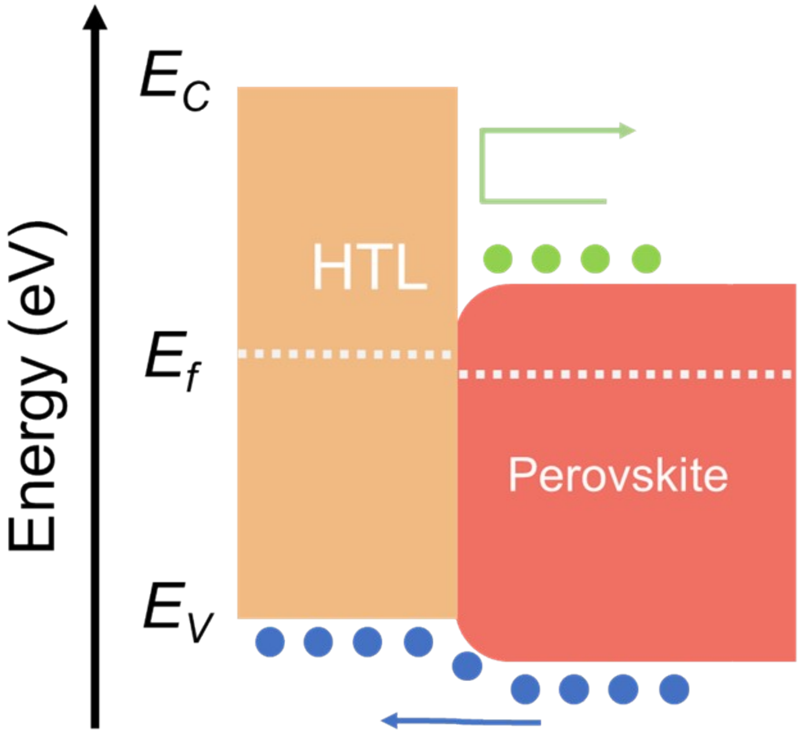

Figure S17: Illustrated energy level alignment at HTL/perovskite interface after 4F-BPA was introduced as DMB.

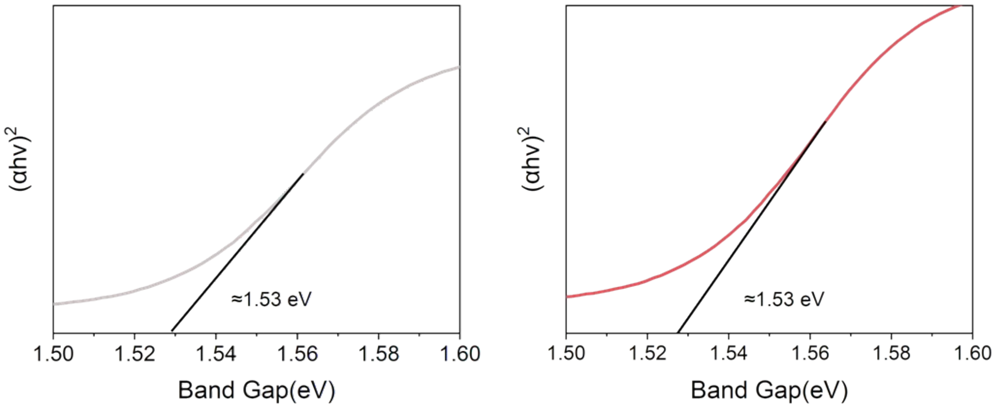

Figure S18: UV-vis spectra for the devices w/&w/o 4F-BPA as DMB

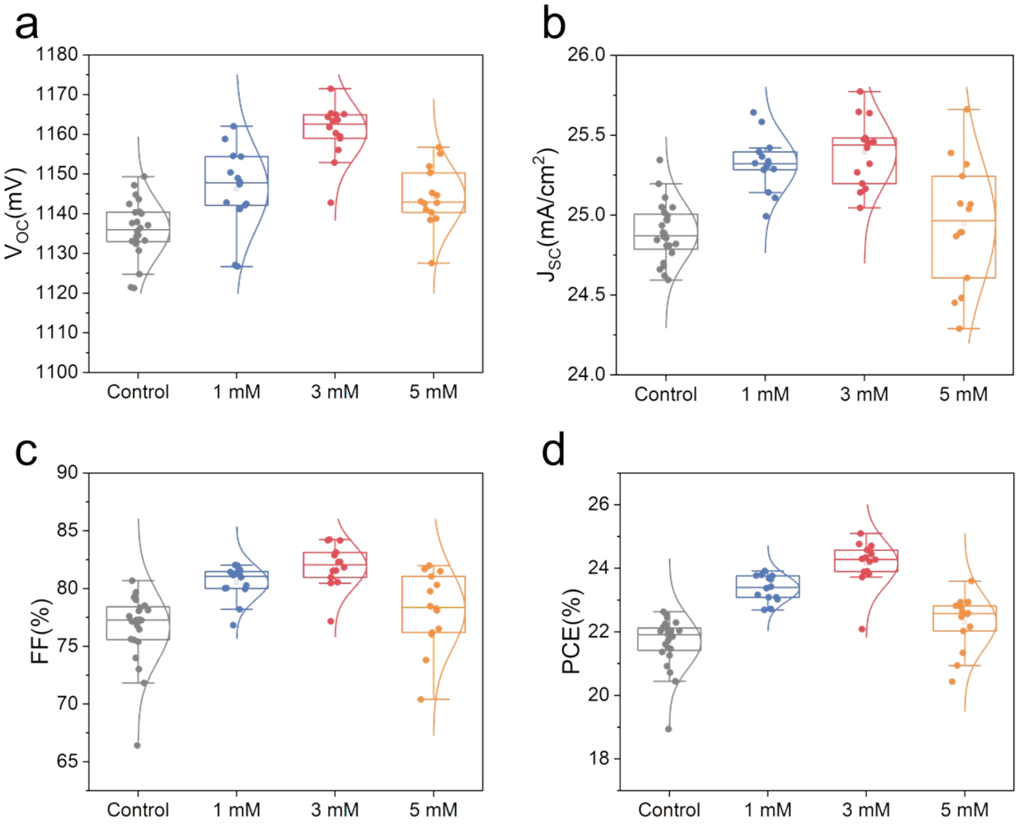

Figure S19: PV performance for devices with 4F-BPA as DMB in various concentrations. a) V_{OC}, b) J_{SC}, c) FF, d) PCE.

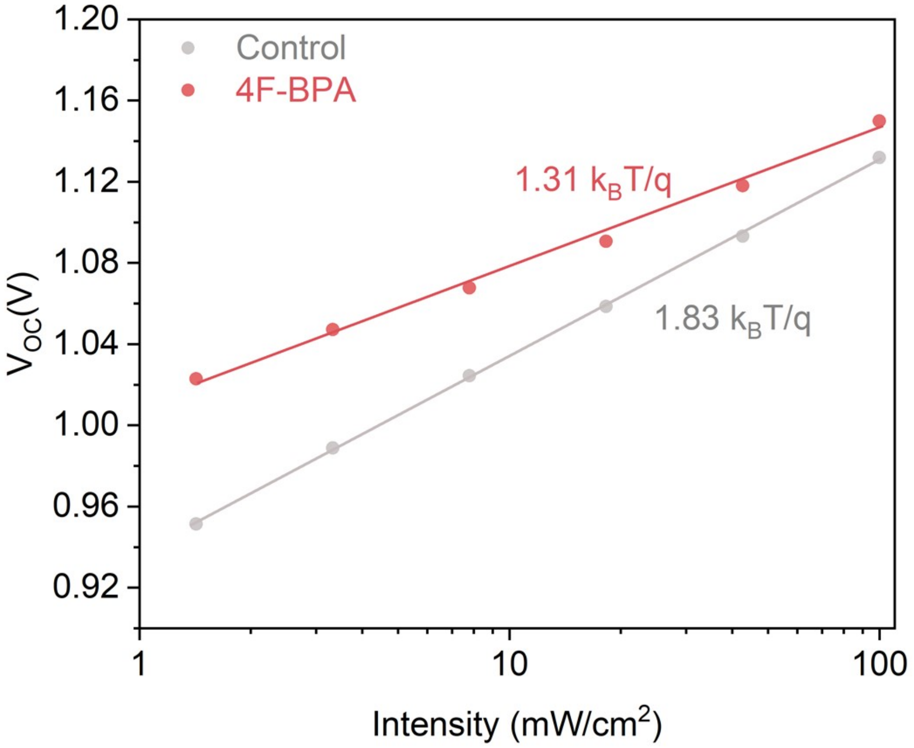

Fig S20: Ideal factors for devices w/&w/o 4F-BPA at HTL.

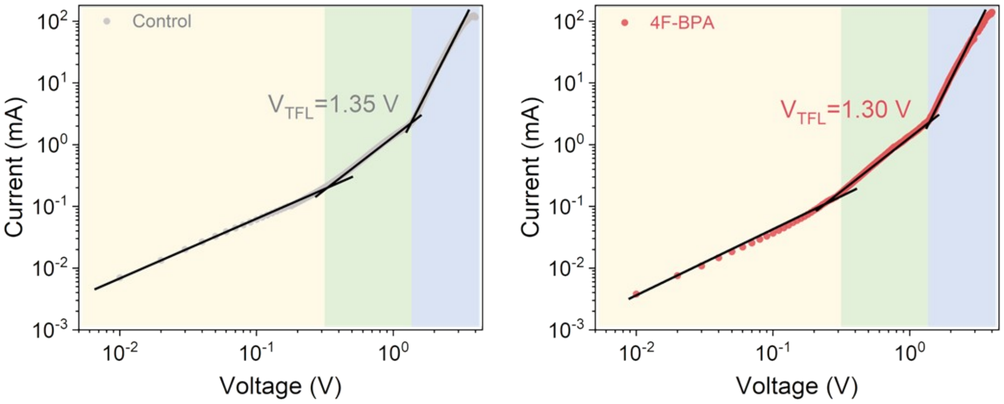

Fig S21: SCLC fitting curves for devices w/&w/o 4F-BPA at HTL.

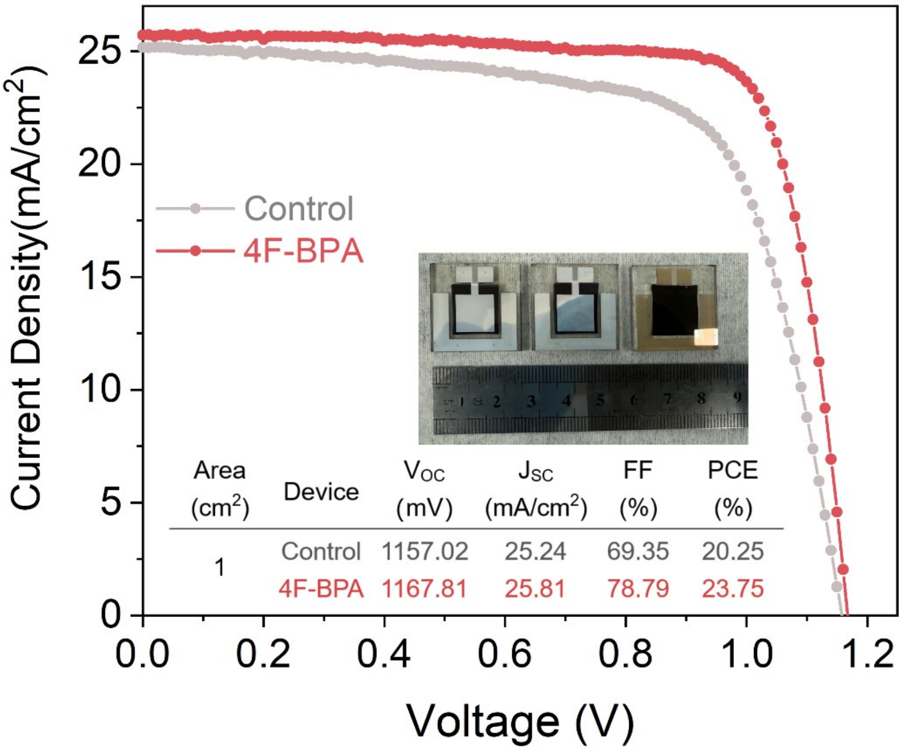

Area (cm^2)	Device	V_{OC} (mV)	J_{SC} (mA/cm^2)	FF (%)	PCE (%)
1	Control	1157.02	25.24	69.35	20.25
	4F-BPA	1167.81	25.81	78.79	23.75

Figure S22: JV curves for the 1 cm^2 inverted PSCs.

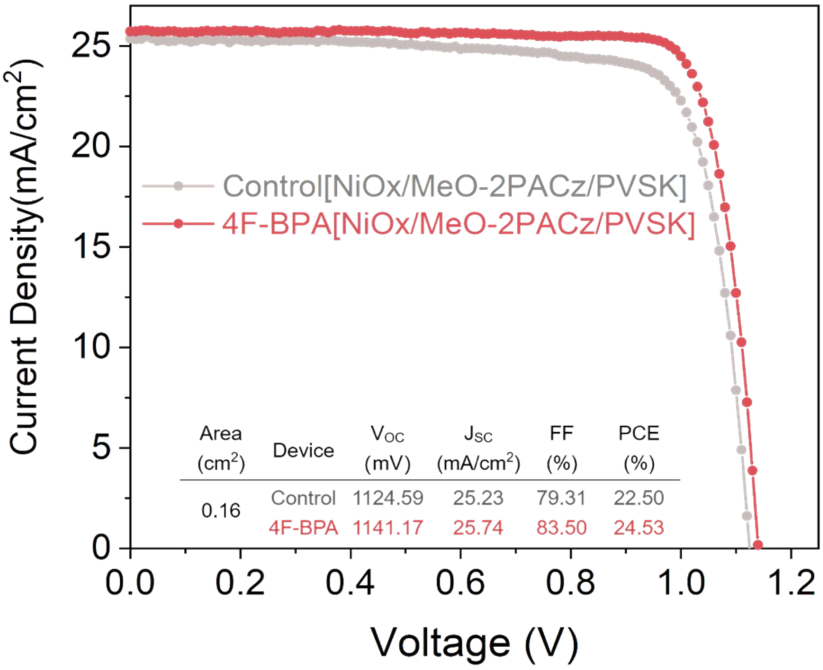

Area (cm^2)	Device	V_{OC} (mV)	J_{SC} (mA/cm^2)	FF (%)	PCE (%)
0.16	Control	1124.59	25.23	79.31	22.50
	4F-BPA	1141.17	25.74	83.50	24.53

Figure S23: JV curves for the inverted PSCs with NiO/MeO-2PACz as HTL.

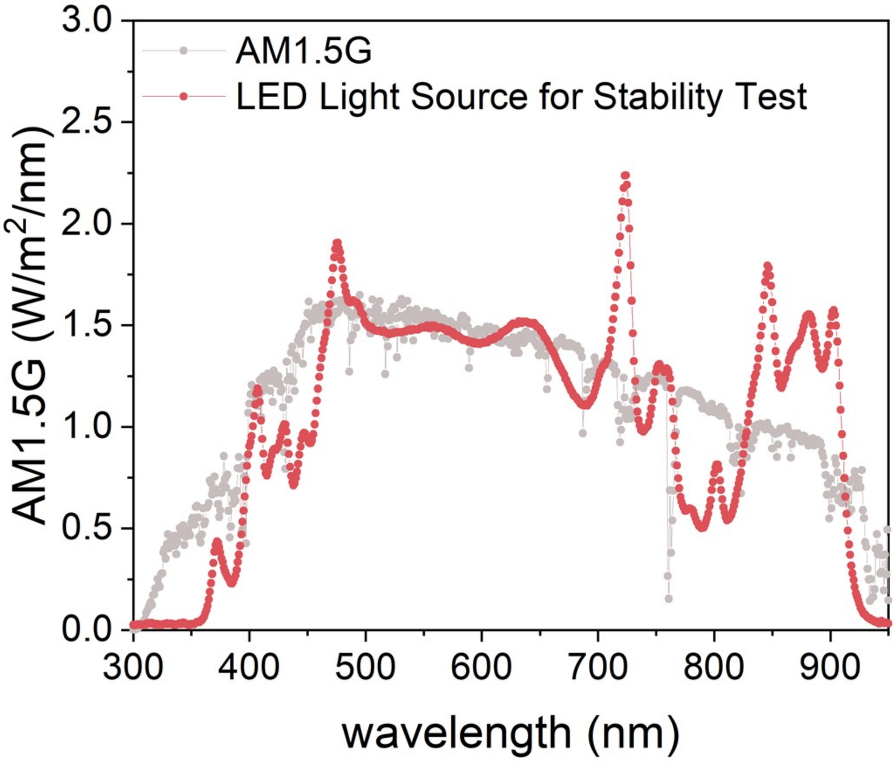

Fig S24 Comparison for the light spectrum used in stability test (LED) and AM 1.5G

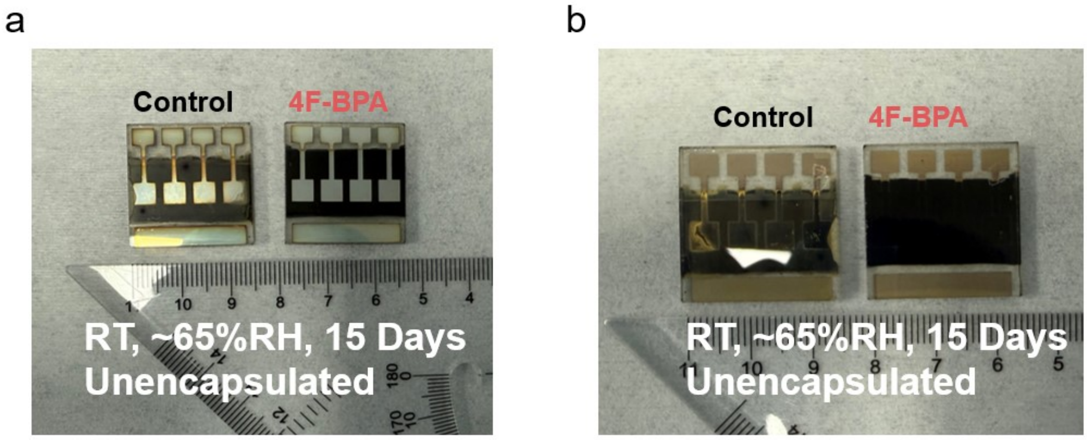

Figure S25: Long-term storage test for unencapsulated PSC device with C_{60}/22 nm ALD-SnO_2 as ETL, under RT, ~65% RH for 15 days. a) the front (Ag contact) side and b) the back (glass) side of the aged device.

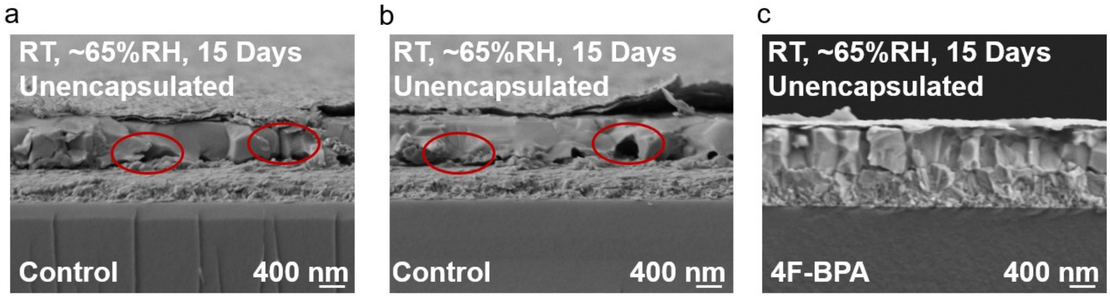

Figure S26: Cross-sectional SEM image for unencapsulated PSC device with C_{60}/22 nm ALD-SnO_2 as ETL, under RT, ~65% RH for 15 days. a) and b) for the control device, c) for the device treated by 4F-BPA as DMB. Cracks, voids and grain boundaries were marked by red circles. d) illustrated mechanism for 4F-BPA as DMB improved the device stability.

Supplementary Table S1:

Recent Inverted PSCs with active area similar to 0.16 cm^2 (2022-2024)

Area (cm^2)	Perovskite	V_{OC} (mV)	FF (%)	PCE (%)	Ref
0.16	$Cs_{0.05}FA_{0.79}MA_{0.16}PbBr_{0.51}I_{2.49}$	1100	78	18.38	*Solar RRL* [7]
0.16	$FAPbI_3$	1180	82	25.00	*Energy Environ. Sci* [8]
0.16	$FAPbI_3$	1180	83	25.10	*Science*[9]
0.16	**$Cs_{0.05}MA_{0.1}FA_{0.85}PbI_3$**	**1161**	**84.23**	**25.10**	**This work**

Supplementary Table S2:

Recent Inverted PSCs with NiOx/SAM as HTL (2023-2024)

HTL	Eg	V_{OC} (mV)	FF (%)	$\frac{VOC \times FF}{S-Q \text{ Limit}}$	PCE (%)	Ref
ITO/NiOx/MeO-4PADBC	1.53	1.19	85	0.89	25.6	Science[10]
ITO/NiOx/Me-4PACz	1.52	1.16	84	0.86	25.6	Science[11]
FTO/NiOx/Me-4PACz	1.53	1.16	83	0.85	24.5	Science[12]
ITO/NiOx/Co-SAM	1.55	1.175	82.54	0.84	25.09	Adv. Mater.[13]
ITO/NiOx/TBT-BA	1.56	1.19	83.7	0.85	24.8	Adv. Energy. Mater.[14]
ITO/NiOx/BTF14	1.55	1.17	83.09	0.84	24.2	Adv. Funct. Mater.[15]
ITO/NiOx/Me-4PACz	1.55	1.14	83.88	0.83	22.29	*App. Phy. Let.*[16]
NiOx/Mix SAM	**1.53**	**1.16**	**84.23**	**0.86**	**25.10**	**This work**

*The idealized V_{OC}×FF in S-Q limit value for 1.53 eV semi-conductor was 1261 mV×90.2%

Supplementary Table S3:

Detailed Photovoltaic Parameters for PSCs with Various Concentrations of 4F-BPA as DMB

Device		V_{OC} (mV)	J_{SC} (mA/cm^2)	FF (%)	PCE (%)
Control	Average	1136.04±7.13	24.89±0.18	76.65±3.02	21.67±0.80
	Champion	1149.32	25.3435	80.68	22.63
1 mM	Average	1146.20±10.35	25.32±0.17	80.51±1.48	23.37±0.41
	Champion	1162.02	25.64	82.02	23.91
3 mM	Average	1160.72±6.85	25.39±0.21	81.94±1.88	24.15±0.71
	Champion	1171.48	25.77	84.23	25.10
5 mM	Average	1144.17±7.58	24.95±0.39	78.14±3.33	22.30±0.86
	Champion	1156.74	25.6603	81.98	23.59

Supplementary Table S4:

Comparison between DMB strategy and other typical interfacial modification strategies

Strategy	Material	Efficiency	Passivation ($\frac{VOC \times FF}{S-Q}$)	Stability (ISOS-L)	Cost* ($/g)	Ref
Molecular Bridge (MB)	PFN-Br	22.5%	0.79	-	4515.2	J. Mat. Chem. A[17]
MB & passivator	PFN-Br & IAI	23.74%	0.82	T80=680h,2I, unencapsulated	4515.2 +53.82	Research[18]
Customized SAM	MPA-CPA	25.4%	0.88	90%, 3I, encapsulated	935.60	Science[19]
	MeO-4PADCB	25.6%	0.89	>90%,3I, encapsulated	970.95	Science[10]
DMB	**4F-BPA**	**25.1%**	**0.86**	**87.1%,1I, unencapsulated**	**224.3**	**This work**

*The cost was mainly collected from Sigma-Aldrich, TCI, and Ningbo Borun Co:

https://www.sigmaaldrich.cn/

https://www.tcichemicals.com/

https://www.chemborun.com/

Reference:

[1] H. Chen, C. Liu, J. Xu, A. Maxwell, W. Zhou, Y. Yang, Q. Zhou, A. S. R. Bati, H. Wan, Z. Wang, L. Zeng, J. Wang, P. Serles, Y. Liu, S. Teale, Y. Liu, M. I. Saidaminov, M. Li, N. Rolston, S. Hoogland, T. Filleter, M. G. Kanatzidis, B. Chen, Z. Ning, E. H. Sargent, *Science* **2024**, *384*, 189.

[2] C. Liu, Y. Yang, H. Chen, J. Xu, A. Liu, A. S. R. Bati, H. Zhu, L. Grater, S. S. Hadke, C. Huang, V. K. Sangwan, T. Cai, D. Shin, L. X. Chen, M. C. Hersam, C. A. Mirkin, B. Chen, M. G. Kanatzidis, E. H. Sargent, *Science* **2023**, *382*, 810.

[3] J. Hutter, M. Iannuzzi, F. Schiffmann, J. VandeVondele, *WIREs Comput. Mol. Sci.* **2014**, *4*, 15.

[4] B. G. LIPPERT, J. HUTTER, M. PARRINELLO, *Molecular Physics* **1997**, *92*, 477.

[5] J. VandeVondele, J. Hutter, *J. Chem. Phys.* **2007**, *127*, 114105.

[6] S. Goedecker, M. Teter, J. Hutter, *Phys. Rev. B* **1996**, *54*, 1703.

[7] Q. Liu, P. Lv, Y. Wang, Y. Zhu, M. Hu, F. Huang, Y.-B. Cheng, J. Lu, *Solar RRL* **2022**, *6*, 2200232.

[8] B. Tian, P. Zhang, T. Liu, W. Chu, Y. Long, P. Xu, Y. Jiang, J. Zhang, Y. Tang, X. Sun, R. Nie, X. Zhao, W. Guo, Z. Zhang, *Energy Environ. Sci.* **2024**, 10.1039.D4EE02803A.

[9] X. Zhao, P. Zhang, T. Liu, B. Tian, Y. Jiang, J. Zhang, Y. Tang, B. Li, M. Xue, W. Zhang, Z. Zhang, W. Guo, *Science* **2024**, *385*, 433.

[10] Z. Li, X. Sun, X. Zheng, B. Li, D. Gao, S. Zhang, X. Wu, S. Li, J. Gong, J. M. Luther, *Science* **2023**, *382*, 284.

[11] H. Gao, K. Xiao, R. Lin, S. Zhao, W. Wang, S. Dayneko, C. Duan, C. Ji, H. Sun, A. D. Bui, C. Liu, J. Wen, W. Kong, H. Luo, X. Zheng, Z. Liu, H. Nguyen, J. Xie, L. Li, M. I. Saidaminov, H. Tan, *Science* **2024**, *383*, 855.

[12] C. Li, X. Wang, E. Bi, F. Jiang, S. M. Park, Y. Li, L. Chen, Z. Wang, L. Zeng, H. Chen, Y. Liu, C. R. Grice, A. Abudulimu, J. Chung, Y. Xian, T. Zhu, H. Lai, B. Chen, R. J. Ellingson, F. Fu, D. S. Ginger, Z. Song, E. H. Sargent, Y. Yan, *Science*

2023, *379*, 690.

[13] Q. Cao, T. Wang, X. Pu, X. He, M. Xiao, H. Chen, L. Zhuang, Q. Wei, H. Loi, P. Guo, B. Kang, G. Feng, J. Zhuang, G. Feng, X. Li, F. Yan, *Advanced Materials* **2024**, *36*, 2311970.

[14] Y. Zhou, X. Huang, J. Zhang, L. Zhang, H. Wu, Y. Zhou, Y. Wang, Y. Wang, W. Fu, H. Chen, *Advanced Energy Materials* **2024**, *14*, 2400616.

[15] X. Sun, C. Zhang, D. Gao, S. Zhang, B. Li, J. Gong, S. Li, S. Xiao, Z. Zhu, Z. Li, *Adv Funct Materials* **2024**, *34*, 2315157.

[16] J. Wei, X. Wang, H. Yang, J. Guo, T. Li, C. Zhu, F. Hou, *Applied Physics Letters* **2024**, *125*, 142109.

[17] S.-C. Liu, H.-Y. Lin, S.-E. Hsu, D.-T. Wu, S. Sathasivam, M. Daboczi, H.-J. Hsieh, C.-S. Zeng, T.-G. Hsu, S. Eslava, T. J. Macdonald, C.-T. Lin, *J. Mater. Chem. A* **2024**, *12*, 2856.

[18] B. Zhou, C. Shang, C. Wang, D. Qu, J. Qiao, X. Zhang, W. Zhao, R. Han, S. Dong, Y. Xue, Y. Ke, F. Ye, X. Yang, Y. Tu, W. Huang, *Research* **2024**, research.0309.

[19] S. Zhang, F. Ye, X. Wang, R. Chen, H. Zhang, L. Zhan, X. Jiang, Y. Li, X. Ji, S. Liu, M. Yu, F. Yu, Y. Zhang, R. Wu, Z. Liu, Z. Ning, D. Neher, L. Han, Y. Lin, H. Tian, W. Chen, M. Stolterfoht, L. Zhang, W.-H. Zhu, Y. Wu, *Science* **2023**, *380*, 404.